Available online at www.sciencedirect.com
SCIENCE DIRECT
Journal of Power Sources 150 (2005) 86–100
JOURNAL OF POWER SOURCES
www.elsevier.com/locate/jpowsour

Behaviour of various glass–ceramic sealants with ferritic steels under simulated SOFC stack conditions

V.A.C. Haanappel [a,*], V. Shemet [a], S.M. Gross [b], Th. Koppitz [b], N.H. Menzler [a], M. Zahid [a], W.J. Quadakkers [a]

[a] *Institute for Materials and Processes in Energy Systems, Forschungszentrum Jülich, Jülich 52425, Germany*
[b] *Central Department of Technology, Forschungszentrum Jülich, Jülich 52425, Germany*

Received 11 October 2004; received in revised form 4 February 2005; accepted 7 February 2005
Available online 5 April 2005

Abstract

The suitability of various combinations of glass–ceramic sealants with high-chromium ferritic steels under conditions simulating SOFC stacks has been evaluated, i.e. three glass–ceramic sealants and seven types of ferritic steels. The test method used is based on test samples consisting of two metallic sheets, joined together with a glass–ceramic sealant. The outer side of the specimens was exposed to air for 400 h at 800 °C, whereas the inner side was exposed to hydrogen saturated with 3 vol.% water vapour. In particular, attention is paid to the influence of small amounts of additives to both the glass–ceramic sealant and the steel on the electrical and chemical behaviour of the specimens.

Under experimental conditions simulating SOFC stacks, it appeared that excessive internal Cr oxidation of the ferritic steels, sometimes accompanied by external Fe-oxide formation, only occurred in the case of glass–ceramics containing minor amounts of PbO. This internal oxidation finally resulted in a volume change of the ferritic steel, which was manifested in bulging of the steel. As a consequence, the glass–ceramic was pushed away from the steel surface and crack formation at the glass–ceramic–steel interface occurred. The rate of corrosion attack strongly depended on the detailed steel composition. Increasing Si content apparently increased the rate of the corrosion attack, and thus possibly decreasing the time for the occurrence of short-circuiting.
© 2005 Elsevier B.V. All rights reserved.

Keywords: SOFC; Glass–ceramic sealants; Interconnect materials; High-chromium ferritic steels; Chemical interaction; Corrosion

1. Introduction

In planar type SOFC devices, glass–ceramic-based materials from the BCAS ($BaO–CaO–Al_2O_3–SiO_2$) system are often used for joining dissimilar materials, i.e. ceramic cells, metallic manifolds, and metallic interconnects [1–6]. These joints should be both gastight and electrically insulating, which implies that the sealants should separate:

- the fuel gas in the inlet and outlet channels from the oxidising environment, i.e. the cathode compartment and outer side of the stack (ambient atmosphere), and
- the oxidising gas in the inlet and outlet channels from the anode compartment (fuel gas) and the outer ambient environment.

In addition to these properties, the glass sealant should possess a thermal expansion coefficient which is similar to that of the material to be joined. It should also exhibit long-term stability under oxidising, reducing, as well as dual environmental conditions at high temperatures as well as chemical compatibility with the joined materials. Also, properties like viscosity at the joining temperature, wetting ability of the joined components, and leakage rates of the sealant have to be optimised [1–3,7]. In order to fulfil the necessary requirements, several additives are frequently used to influence the chemical and physical properties of the glass sealant. An overview of the effects achieved by small

* Corresponding author. Tel.: +49 2461 614656; fax: +49 2461 616770.
E-mail address: v.haanappel@fz-juelich.de (V.A.C. Haanappel).

0378-7753/$ – see front matter © 2005 Elsevier B.V. All rights reserved.
doi:10.1016/j.jpowsour.2005.02.015

Table 1
Effects of the presence of small amounts of additives in the glass–ceramic sealant [7]

Compounds	Effects
La_2O_3, Nd_2O_3, Y_2O_3	Increased thermal expansion coefficient, α, T_g, T_m, controlling viscosity
B_2O_3	Improves flux; reduces α, surface tension
ZnO, PbO	Improves flux, reducing agent
Al_2O_3	Improves flux, retarding crystallisation
Cr_2O_3, V_2O_5	Reduces surface tension
NiO, CuO, CoO, MnO	Improves adhesion
TiO_2, ZrO_2, SrO	Promotes crystallisation
Sb_2O_5	Oxidising agent

amounts of additives is given in Table 1 [7]. For instance, ZnO and PbO can be added as a reducing agent, thus improving the adhesion between the steel and the glass–ceramic sealant [8].

The main properties required for the interconnect materials are [9]:

- a sufficient chemical resistance to a dual atmosphere with, on the cathode side, an oxidising environment and on the anode side a reducing environment;
- a thermal expansion coefficient adapted to the other components;
- a sufficiently high electronic conductivity of the bulk material as well as of the oxide scale formed;
- satisfactory compatibility with the glass or glass–ceramic sealants.

Taking these requirements into account, potential candidates for the interconnect are based on ferritic steels with a chromium concentration of at least 17 wt.% [9]. The latter ensures the formation of a continuous and protective Cr-based oxide scale during high-temperature exposure. Generally, these types of steels also contain small amounts of Si and Al to keep the oxygen concentration in the steel at a sufficiently low level during production.

A recent study based on a fast-screening test exposing various glass–ceramic sealant/ferritic steel combinations to high temperatures in a hydrogen/water vapour mixture already revealed that certain combinations induced severe degradation of the ferritic steel [10]. In addition to this, experiments were initiated with sandwich samples tested under conditions simulating SOFC stack conditions more closely.

In the present the interaction of various glass–ceramic sealants with a number of ferritic steels under simulated conditions relevant for SOFC stacks are evaluated. The experimental method is based on test samples consisting of two metallic sheets joined by a glass–ceramic sealant [11]. The outer side of the sample is exposed to ambient atmosphere, whereas the inner side is exposed to hydrogen saturated with 3 vol.% of water vapour.

Special emphasis is put on the influence of small amounts of additives in both the glass–ceramic sealant and the steel on the electrical and chemical properties of the specimens.

Table 2
Chemical composition of the steels used (wt.%)

Steel	Fe	Cr	Mn	Ti	Si	Al	Re-el.	Ni
T-1	Balance	22.6	0.4	0.06	0.1	0.1	La-0.1	0.2
T-2	Balance	23.3	0.4	0.05	<0.01	<0.01	La-0.1	–
T-3	Balance	22.1	0.5	–	0.4	0.2	Zr-0.1	0.3
T-4	Balance	22.1	0.5	0.05	0.02	0.02	La-0.05	0.02
T-5	Balance	22.1	0.4	0.05	0.1	<0.01	La-0.1	–
T-6	Balance	22.0	0.4	0.05	<0.01	0.1	La-0.1	–
T-7	Balance	22.7	0.4	0.04	<0.01	<0.01	La-0.05	–

2. Experimental

2.1. Materials

The test samples consisted of two metallic sheets of a ferritic steel. The sheets with a thickness of 2.0 mm were cut into 50 mm × 50 mm squares, whereby one sheet contained a small hole in the centre (diameter: 10 mm) allowing the desired gas composition to reach the inner part of the sample. The surfaces of the steel sheets were ground and ultrasonically cleaned with ethanol and acetone. Table 2 shows the chemical compositions of the various model steels tested.

The glass–ceramic sealants used in this study are based on mixtures of Al_2O_3, SiO_2, CaO, and BaO. They additionally contain minor amounts of transition metal oxides to optimise the SOFC-relevant physical and chemical properties [7]. The chemical compositions of the various glass–ceramic sealants used are given in Table 3. The glass paste containing an organic binder was applied by a robot dispenser to the circumference of one of the sheets in the sandwich sample.

2.2. Electrical resistance measurements

In order to measure the electrical resistance of the sample, each sheet was connected to two Pt wires, one to apply the external voltage over the glass sealant and the other to measure the current density. The samples were placed on top of a hermetically sealed alumina housing, which contained four gas outlets. With this set-up a maximum of four samples could be tested simultaneously. A silver gasket was used to obtain gas tightness between the alumina housing and the sample. The sandwich samples were placed into the furnace, each sample being loaded by a weight of about 300 g. A schematic set-up of the test unit is depicted in Fig. 1.

For the joining of the metallic sheets and crystallisation of the glass–ceramic sealant the samples were heated in air to 850 °C at a heating rate of 1 °C min^{-1}. After reaching 850 °C, a dwell time was set. This was followed by cooling down to

Table 3
Chemical composition of the various glass–ceramic sealants used (wt.%)

Glass sealant	SiO_2	CaO	BaO	Small additives
G73	34.7	8.6	41.4	Al_2O_3, B_2O_3, ZnO, PbO, V_2O_5
G75	35.0	8.5	42.8	Al_2O_3, B_2O_3, PbO, V_2O_5
G76	36.3	8.6	42.1	Al_2O_3, B_2O_3, ZnO, V_2O_5

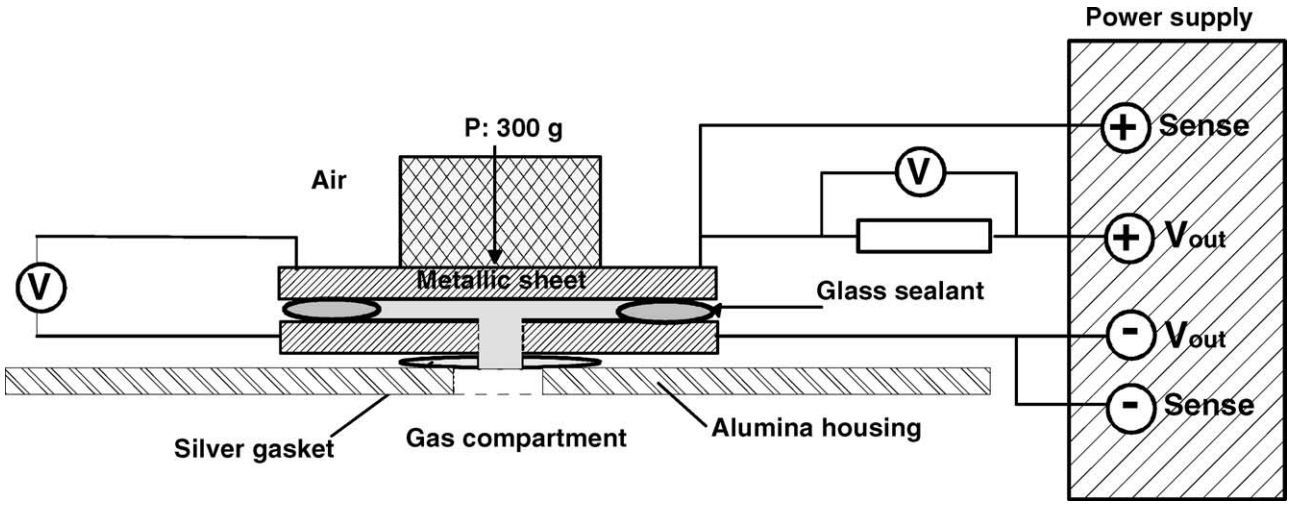

Fig. 1. Schematic view of the experimental set-up for electrical resistance measurements during high-temperature exposure in dual atmospheres.

800 °C at 1 °C min^{-1}. During this process organic solvents were removed, the glass was softened and a chemical interaction occurred between the glass sealant and the steel resulting in chemical bonding [8]. After reaching the desired test temperature of 800 °C, the inner part of the alumina housing was flushed (100 ml min^{-1} ATP) with the desired gas composition: hydrogen saturated with 3 vol.% H_2O on the inner side, and air on the outer part of the samples. An external voltage of 800 mV, typically prevailing in SOFC stacks, was applied. The electrical resistance measurements were based on DC methods using a current-control power supply type Gossen 24K32R4 (Gossen-Metrawatt GmbH, Germany) and a computer-controlled data acquisition system, including a datalogger type NetDAQ 2640A (Fluke, The Netherlands). Current density, external voltage, and consequently the overall electrical resistance of the sample were monitored continuously. After the total exposure time, the samples were cooled down to ambient temperature at a rate of 1 °C min^{-1}. During cooling the inner part of the samples was flushed with argon.

2.3. Microstructural characterisation

Scanning electron microscopy (SEM) analyses of the surface morphology and cross-sections of the specimens tested was performed using a LEO 1530 electron microscope equipped with an EDX analysis system.

3. Results

3.1. Electrical resistance measurements

Fig. 2a–d shows results from resistance measurements with various combinations of steel/glass sealants. It is found that under the given experimental conditions, the resistance of sandwich samples with the steel/glass sealant combination T1–G73 (measured twice) substantially decreased after about 60 h of exposure. Generally, this short-circuiting occurred after a short-term increase of the resistance (Fig. 2). The specific resistance of specimen T2–G73 (measured twice) was >10 kΩ m during the whole exposure time. After a few hours of exposure specimen T3–G73 already showed significant fluctuations of the electrical resistance (Fig. 2b). The resistance decreased to values of around 20 Ω m after about 140 h of exposure. During exposure of specimen T4–G73 no obvious decrease of the resistance was measured. For this sample, the specific resistance increased, reaching a maximum value of almost 10 kΩ m after about 50 h. After 170 and 230 h of exposure two specimens of the T5–G73 combination (Fig. 2c) showed a decrease of the resistance to values lower than 1 Ω m. The other specimens, i.e. T6–G73, and T7–G73, did not show any fluctuations of the specific resistance during the total exposure time at 800 °C. Fig. 2d shows the electrical resistance of two samples based on steel T1 and two different glass sealants, i.e. G75 and G76. In this case, after about 220 h of exposure the sandwich sample with the steel/glass sealant combination T1–G75 showed apparent fluctuations of the electrical resistance, finally resulting in short-circuiting. Specimen T1–G76 showed neither fluctuations of the resistance nor any indications of short-circuiting.

3.2. Microstructural analysis

Different locations on the surface area of the specimens were microscopically investigated. To clarify the different locations analysed Fig. 3 shows a schematic view of the sandwich sample, indicating the various analysis areas. Position 1 in Fig. 3 corresponds to the boundary between air, glass sealant, and steel; position 2 corresponds to that between hydrogen, glass sealant and steel and position 3 to the steel surface at the hydrogen side approximately 2–3 mm from the glass sealant.

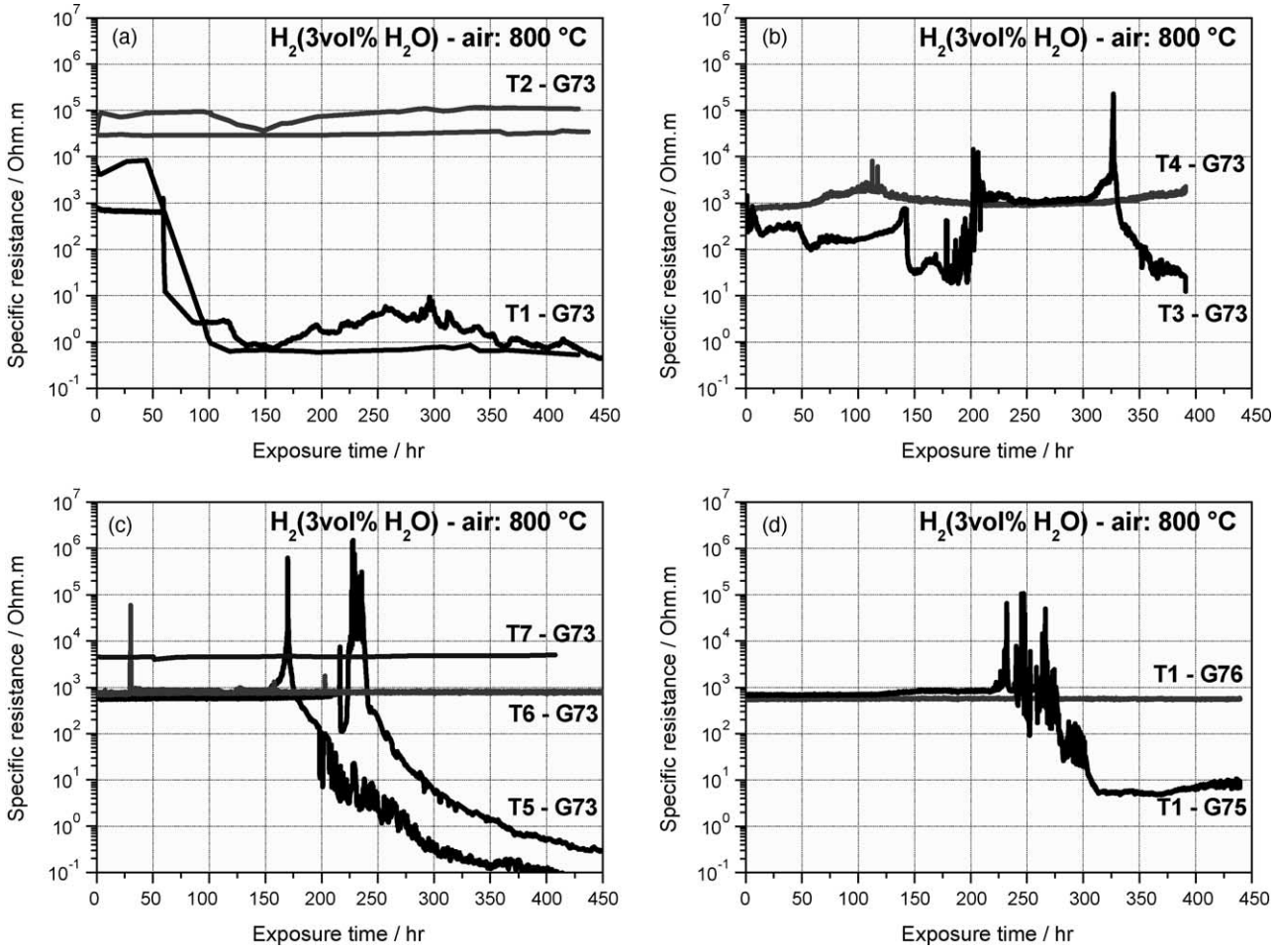

Fig. 2. Specific resistance of various sandwich samples as a function of the exposure time: (a) samples T1–G73, T2–G73; (b) T3–G73, T4–G73; (c) T5–G73, T6–G73, T7–G73; (d) T1–G75, T1–G76. Gas composition: dual atmosphere with hydrogen (3 vol.% H_2O) in the inner part and air at the outer part; temperature: 800 °C; externally applied voltage: 800 mV.

Fig. 4a–d shows micrographs of the surface morphology of specimen T1–G73 near the triple phase boundaries air/glass sealant/steel (Fig. 4a and c) and hydrogen/glass sealant/steel (Fig. 4b and d). Near the glass sealant/steel/air boundary significant amounts of an iron-rich oxide are formed (Fig. 4a). Apart from this corrosion product, the outer edge of the glass sealant was rich in Ba and Cr. On the outer surface of the steel on the air-side, a rather homogeneous oxide layer had formed, which was rich in chromium and manganese. EDX analysis revealed the presence of low concentrations of Pb on the oxide surface in the vicinity of the glass sealant. Fig. 4b shows the three-phase boundary on the hydrogen side. Here, a rather smooth interface between the glass sealant and the steel is observed without the presence of iron-rich oxide products. Furthermore, no substantial Ba-, Cr-rich oxide zone was observed at the edge of the glass sealant at the hydrogen site. White particles, rich in elemental Pb were locally found on the glass edge. On the steel surface, whisker-like oxide products were formed, which were rich in Cr and Mn, or in Fe, Mn, and Cr, as also recently discussed more extensively elsewhere [12–16]. The grinding structure of the underlying steel can still be observed, which implies the formation of a rather thin oxide layer in the hydrogen-based atmosphere.

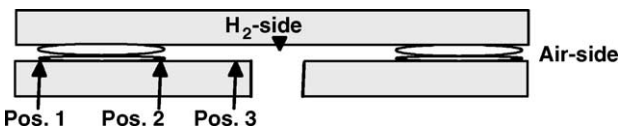

Fig. 3. Schematic view of a sandwich sample (illustrating location of surface and cross-sectional analysis) with hydrogen atmosphere on the inner side and air on the outer side. Position 1 corresponds to the triple phase boundary air/glass–ceramic sealant/steel; position 2 with the triple phase boundary hydrogen/glass–ceramic sealant/steel; and position 3 with the specimen surface outside the vicinity of the glass–ceramic sealant.

Fig. 5a and b shows SEM cross-sections of the specimen T1–G73. Severe material degradation has taken place at the air-side and near the glass sealant/steel edge area, due to extensive interaction between the glass sealant and the steel. EDX analysis revealed the presence of voluminous outwardly growing iron-rich oxide nodules. Internal Cr_2O_3 precipitates were found at the steel grain boundaries as well as in the grains. In this internal oxidation zone, the metallic matrix

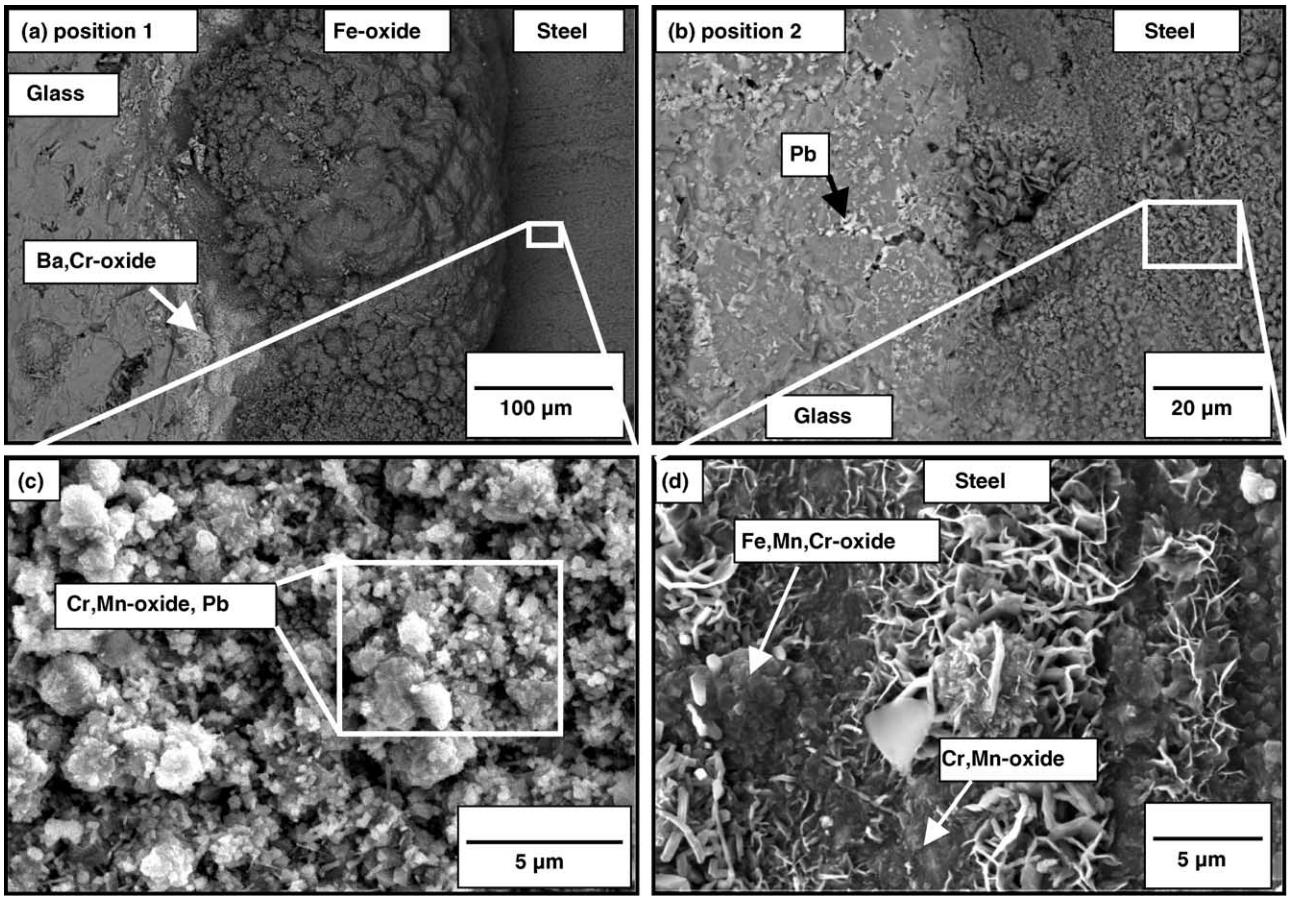

Fig. 4. SEM micrographs of the surface morphology of specimen T1–G73 after exposure for 400 h at 800 °C in a dual atmosphere of hydrogen/air with an externally applied voltage of 800 mV: (a) triple phase boundary air/glass–ceramic sealant/steel (position 1); (b) triple phase boundary hydrogen/glass–ceramic sealant/steel (position 2); (c) higher magnification of the steel surface on the air-side; (d) higher magnification of the steel surface on the hydrogen side.

was depleted in chromium. The glass sealant left behind and located near position 1, formed a bright phase (not depicted in this figure), rich in Ba and Cr. Severe internal oxidation was also found on the hydrogen side. It is important to note that internal oxidation of the steel was not only found on local sites beneath the glass sealant or at the triple phase boundary area, but also on sites at a certain distance from the interface between the glass sealant and the steel. Also at position 2, intergranular and intragranular formation of chromium oxide is observed (Fig. 5b). However, at this position, neither large iron-rich oxide nodules nor the formation of Ba-/Cr-rich oxides were found at the outer zone of the glass sealant.

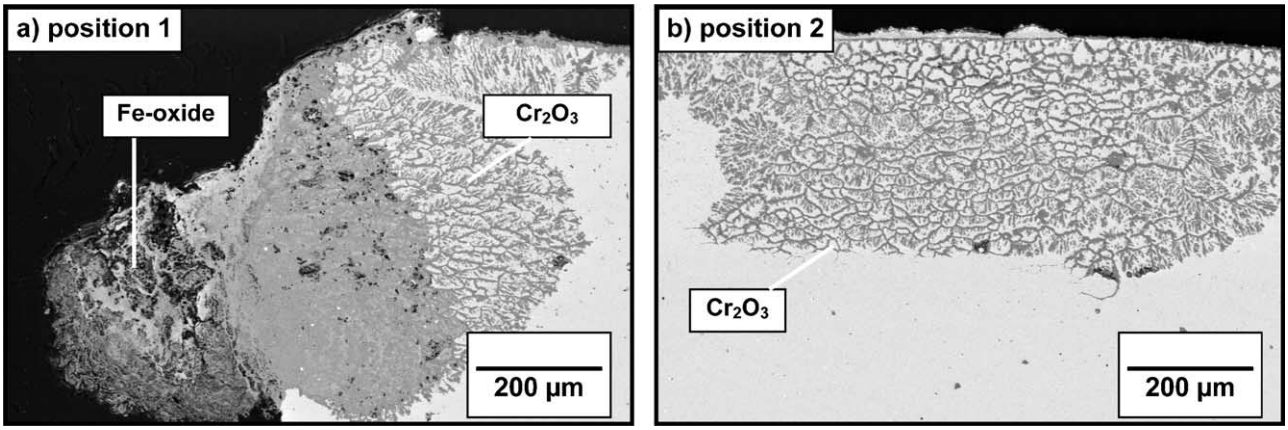

Fig. 5. SEM micrographs of a cross-section of specimen T1–G73 exposed for 400 h at 800 °C in a hydrogen/air dual atmosphere: (a) position 1: air-side; (b) position 2: hydrogen side.

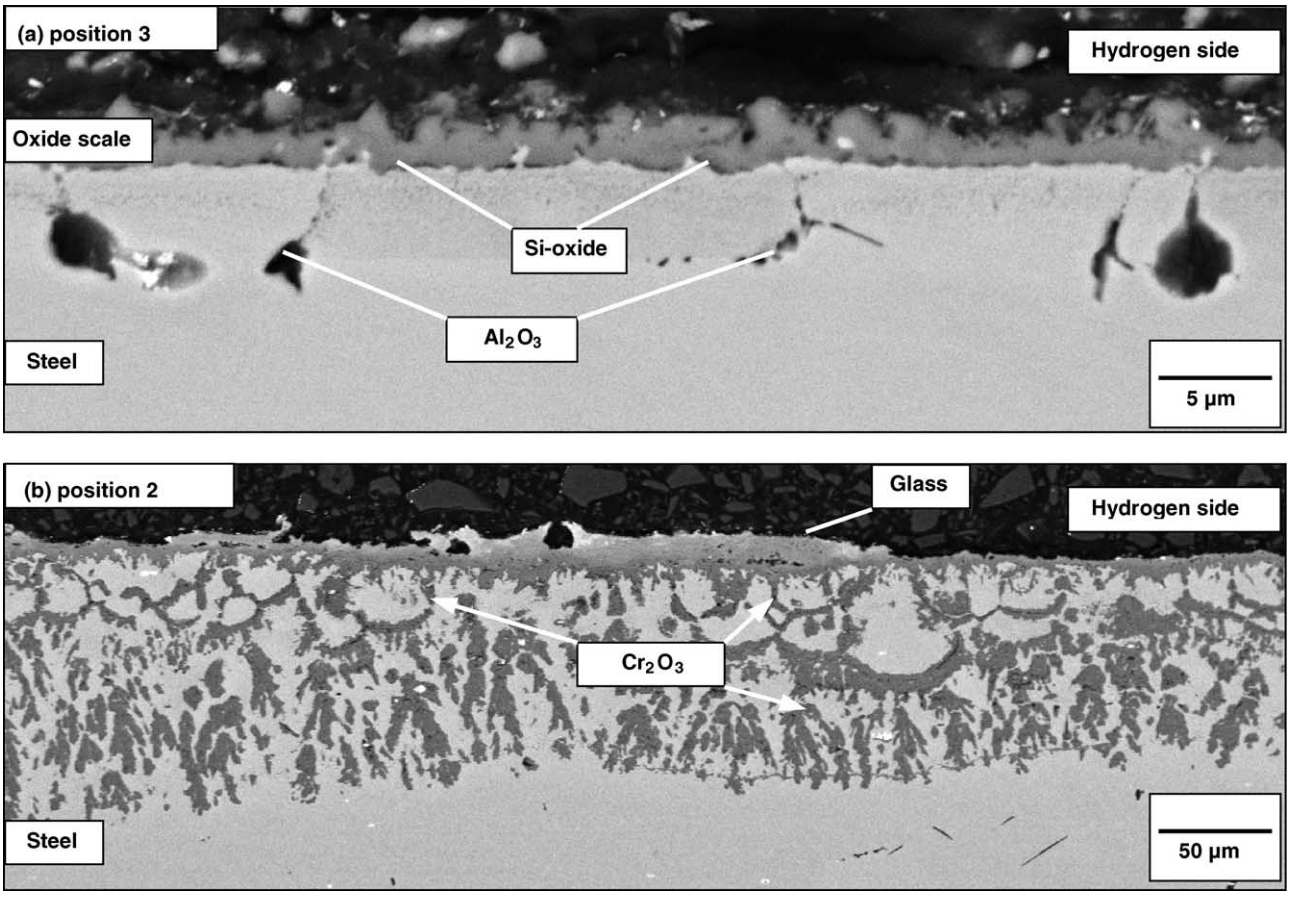

Fig. 6. SEM micrographs of a cross-section of specimen T1–G73 exposed for 400 h at 800 °C in a hydrogen/air dual atmosphere: (a) oxide formation on the steel surface on the hydrogen side without the presence of a glass–ceramic sealant (position 3); (b) oxide growth on the steel surface near position 2.

Fig. 6a shows a higher magnification of the oxide formed on the steel surface further away (position 3) from the glass sealant (Fig. 6a) and the area in which internal oxidation occurred (position 2) (Fig. 6b). On the hydrogen side, only a thin chromium-rich oxide layer is formed (Fig. 6a). Beneath this layer, Si- and Al-rich oxide precipitates are locally found [14]. In the vicinity of position 2 (Fig. 6b) severe internal oxidation occurred. Near the interface between the alloy and the internal oxidation zone, enrichment of Al and sometimes Si was detected locally, whereas in other places internal oxidation was generally characterised by Cr-rich oxide. The maximum internal oxidation depth found under these experimental conditions was about 500 μm.

The surface morphology of specimen T2–G73 after 400 h of exposure at 800 °C in the dual atmosphere hydrogen–air is shown in Fig. 7a–d. On the steel surface exposed to the air-side (Fig. 7a and c) a smooth oxide layer rich in Cr and Mn was formed. Here, residual crystals of the glass–ceramic, rich in Ba, Ca, Si (Pb), and Ba, Cr, and Ba, Ca, Si (Zn, Pb) remained on the steel surface. In contrast to specimen T1–G73, no large iron-rich oxide products were found. On the hydrogen side (Fig. 7b and d), some parts of the glass sealant were spalled off (Fig. 7b), whereas the steel surface near the triple phase boundary (position 2) formed a thin oxide layer (Fig. 7d) rich in Cr, Fe, and Mn, or Cr and Mn. In the cross-sections of specimen T2–G73, neither intergranular nor intragranular oxidation of Cr was found (Fig. 8a and b), and at the three-phase boundary on the air-side (position 1), no voluminous iron-rich oxide nodules were formed. The outer edge of the glass sealant showed a barium- and chromium-rich oxide phase. The oxide scale formed on the steel surface at the hydrogen side (position 3) was rich in chromium. Beneath this oxide layer a zone of homogeneously distributed, very fine titanium oxide precipitates (Fig. 8a) were present. Near the triple phase boundary, at position 2, only a thin oxidation zone, rich in chromium had formed (Fig. 8b). In this case, the maximum internal oxidation depth was about 5 μm. At this position the glass sealant did not form the bright Ba-/Cr-rich oxide, as found on the air-side.

The surface morphology of specimen T3–G73 was similar to that of specimen T1–G73 (see Fig. 4). Also here, large iron-rich oxidation products were formed near the glass edge on the air-side. Metallographic cross-sections revealed similar severe interactions between the glass sealant and the steel as observed in the case of specimen T1–G73 (see Fig. 5). The maximum depth of internal oxidation of the steel was approximately 500 μm, i.e. similar to that found for specimen T1–G73.

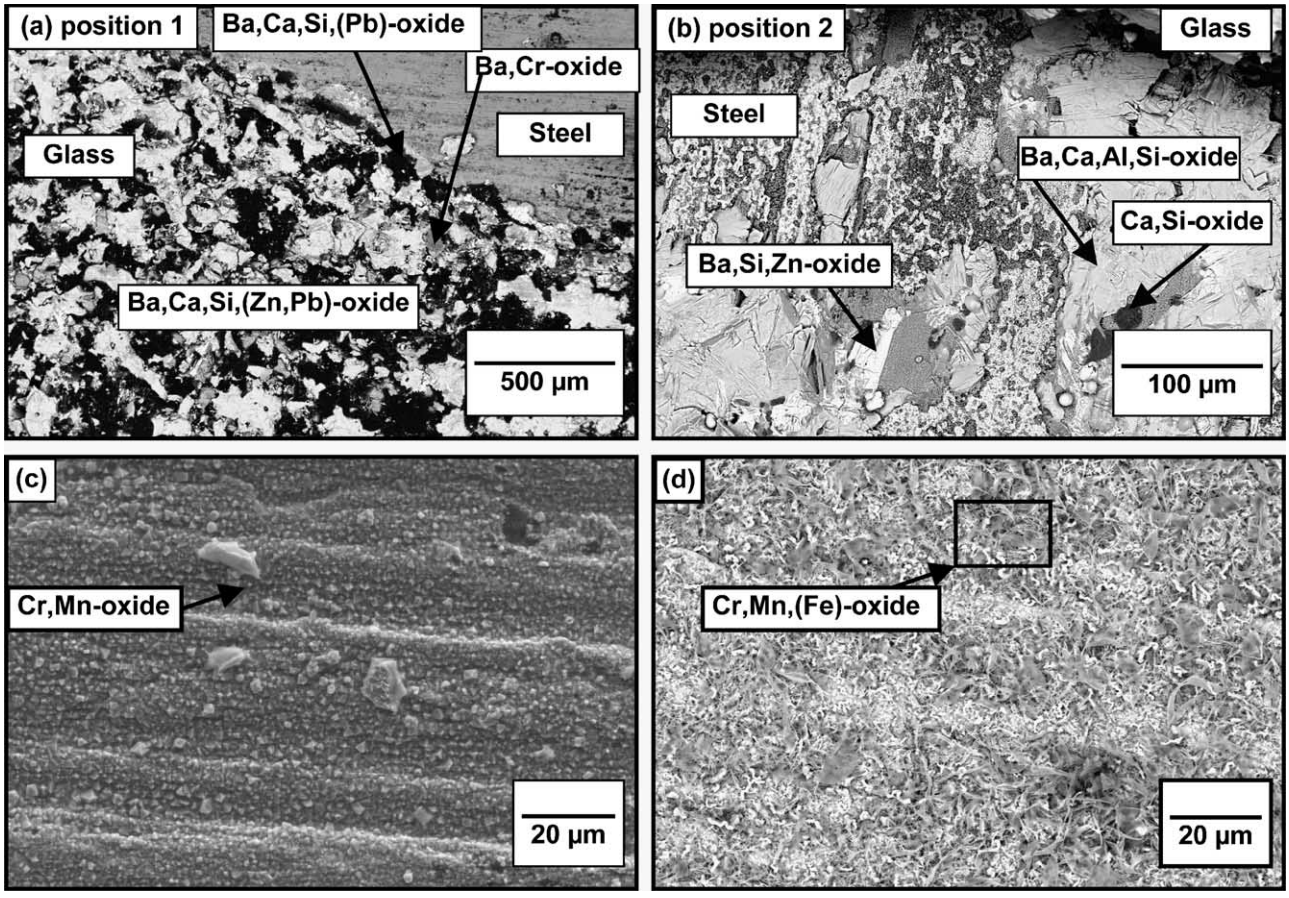

Fig. 7. SEM micrographs of the surface morphology of specimen T2–G73 after exposure for 400 h at 800 °C in a dual atmosphere of hydrogen/air with an externally applied voltage of 800 mV: (a) triple phase boundary air/glass–ceramic sealant/steel (position 1); (b) triple phase boundary hydrogen/glass–ceramic sealant/steel (position 2); (c) steel surface on the air-side; (d) steel surface on the hydrogen side.

After removing specimen T4–G73 from the furnace, no adherence existed any more between the two metallic sheets. Observations revealed that brownish Fe-rich corrosion products were formed along the edges of the glass sealant as well as below the sealant. The surface morphology of the sample was similar to that of specimens T1–G73 and T3–G73. Cross-sectional analysis revealed that for this specimen, the formation of an externally growing iron-containing oxide was less pronounced than that observed on the outer surface of the specimens T1–G73 and T3–G73. Also inter- and intragranular Cr-oxide formation occurred, but was far less pronounced than in the former specimens based on the steels T1 and T2. In this case the depth of internal attack was approximately 30 μm.

Fig. 9 shows the surface morphology of specimen T5–G73 after 400 h of exposure at 800 °C in a hydrogen/air environment. Here, at position 1 corresponding to the glass sealant/steel edge on the air-side, significant amounts of an iron-rich oxide are formed (Fig. 9a). These corrosion products were not found on the hydrogen side (Fig. 9b). Only on the air-side of the glass sealant a bright, Ba-/Cr-rich oxide was formed. A higher magnification of Fig. 9a shows the formation of a rather dense chromium- and manganese-rich oxide layer at the steel surface. Near the glass edge, small amounts of Pb were detected by EDX on the oxide layer. On the hydrogen side, similar oxidation products were formed on the steel surface (Fig. 9d). However, the oxide did not exhibit the dense structure found on the air-side [14]. Cross-sectional observations of this specimen (Fig. 10a and b) revealed similar features to those observed for specimen T1–G73 (Fig. 5). The depth of internal oxidation was about 600 μm. Near the interface between the steel and the internal oxidation zone, internal oxidation products enriched in Al and occasionally in Si and Al were detected.

For specimens T7–G73 (Fig. 11) and T6–G73, similar observations were made as for specimen T2–G73 (see Fig. 7). No voluminous iron-rich oxidation products were formed, neither at the air-side nor on the hydrogen side. Near the air-side the glass sealant showed the formation of a Ba-/Cr-rich oxide zone. In the vicinity of the glass sealant, particles containing elemental Pb were locally found. Fig. 11 shows SEM micrographs of specimen T7–G73 in the region near the glass edge on the air (Fig. 11a) and hydrogen side (Fig. 11b). The bright phases of the glass sealant are rich in Ba and Cr

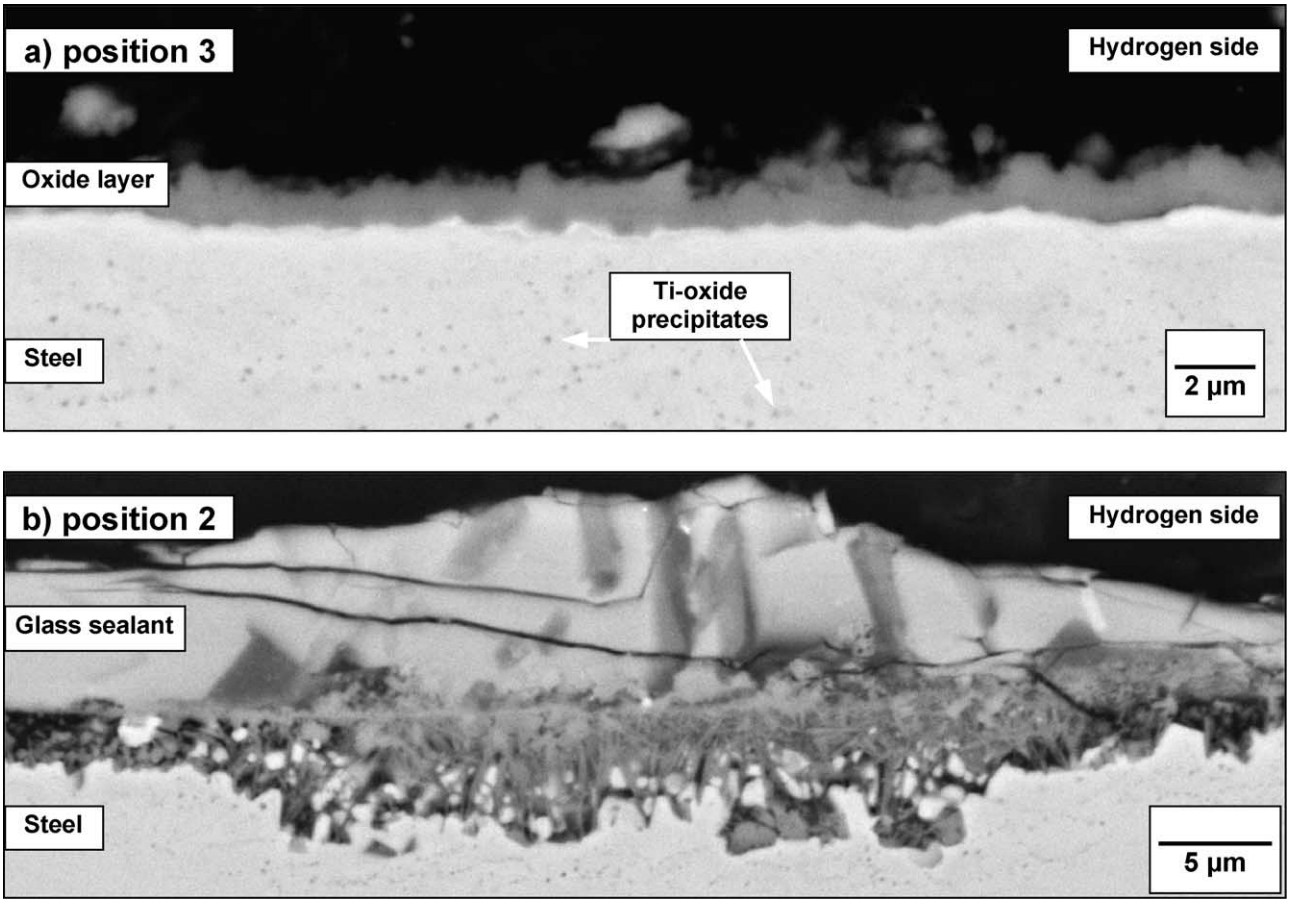

Fig. 8. SEM micrographs of a cross-section of specimen T2–G73 exposed for 400 h at 800 °C in a hydrogen/air dual atmosphere: (a) oxide formation on the steel surface on the hydrogen side without the presence of a glass–ceramic sealant (position 3); (b) internal oxidation on the steel surface near position 2.

(Fig. 11a). Fig. 11c shows bright particles containing elemental Pb. On the hydrogen side, small Fe-rich oxide grains were formed (Fig. 11d). Both specimens neither exhibited severe outward Fe-oxide growth nor severe internal Cr oxidation.

Surface examinations and cross-sectional analysis (Fig. 12a–c) revealed for specimen T1–G75 morphological features similar to those obtained with specimens T1–G73, T3–G73, and T5–G73 (Figs. 4–6, 9 and 10). The depth of internal corrosion attack was about 300 μm. Along one side of the glass sealant/steel interface no adherence between the glass and steel existed any more. Here, severe internal Cr-oxidation as well as outward Fe-oxide growth had taken place. The volume change imparted by the internal oxidation resulted in significant deformation of the steel. As a consequence, the glass sealant was separated from the steel.

After 400 h of exposure under the dual atmosphere the surface morphological features of specimen T1–G76 showed no voluminous Fe-oxide products (Fig. 13a and b). The surface morphology was similar to that of specimens T2–G73, T6–G73, and T7–G73 (Figs. 7, 8 and 11). Cross-sectional analysis revealed no internal oxidation of chromium, neither on the air-side (Fig. 14a) nor on the hydrogen side (Fig. 14b).

4. Discussion

The present study, simulating SOFC stack conditions, has shown that excessive interaction of the glass–ceramic with the interconnect steel can lead to a rapid degradation of stack components due to short-circuiting phenomena. The latter could be shown to be related to voluminous Fe-oxide formation on the steel surface near the boundary between steel, glass–ceramic, and oxidant (air). Due to the high electronic conductivity of the Fe-oxides, especially Fe_3O_4 and FeO, the voluminous oxide growth results in the formation of a "bridge" with extremely small electrical resistance between the adjacent metallic plates and thus in short-circuiting.

The systematic parameter variation in the present study combined with results from other recent investigations [17] revealed the following findings with respect to this undesired degradation phenomenon:

- The voluminous, outward Fe-oxide growth only occurs at the boundary between the oxidant (air), the glass–ceramic, and the steel, and is accompanied by excessive internal oxidation of chromium in the steel.
- Internal oxidation of chromium also occurs at the boundary between the hydrogen-based environment, the

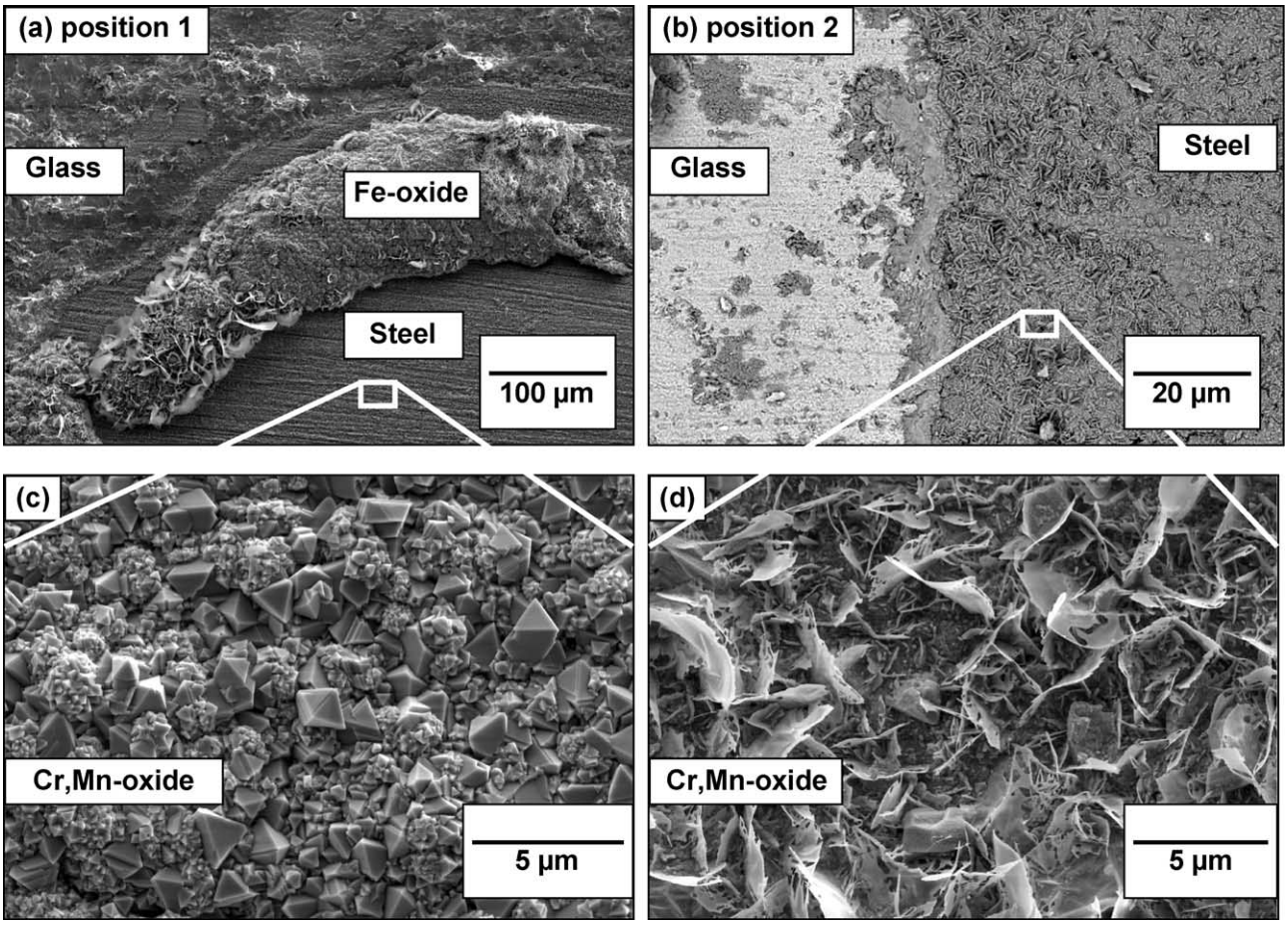

Fig. 9. SEM micrographs of the surface morphology of specimen T5–G73 after exposure for 400 h at 800 °C in a dual atmosphere of hydrogen/air with an externally applied voltage of 800 mV: (a) triple phase boundary air/glass–ceramic sealant/steel (position 1); (b) triple phase boundary hydrogen/glass–ceramic sealant/steel (position 2); (c) higher magnification of the steel surface on the air-side; (d) higher magnification of the steel surface on the hydrogen side.

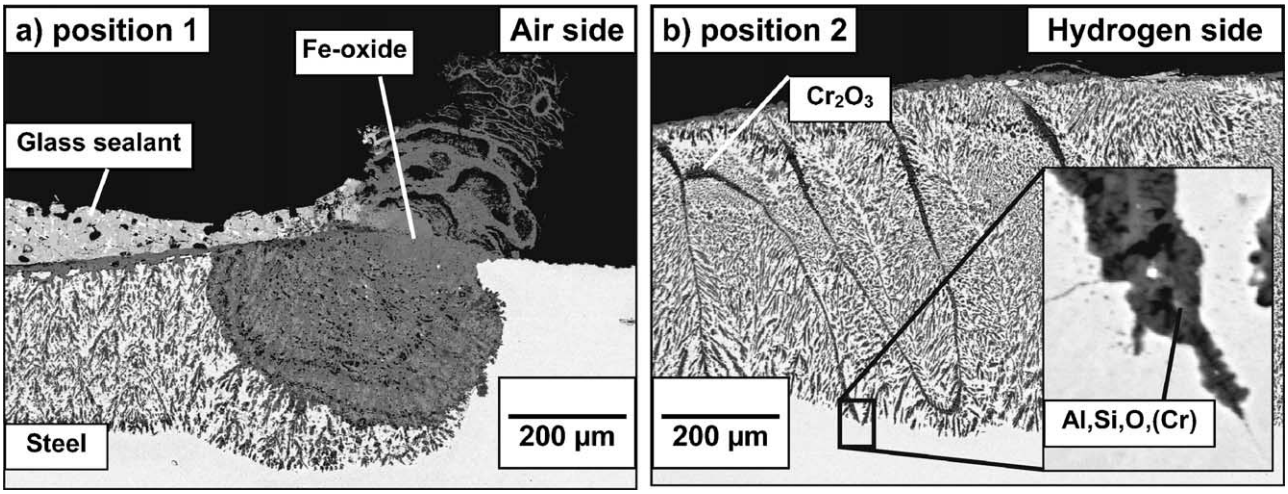

Fig. 10. SEM micrographs of a cross-section of specimen T5–G73 exposed for 400 h at 800 °C in a hydrogen/air dual atmosphere: (a) position 1: air-side; (b) position 2: hydrogen side.

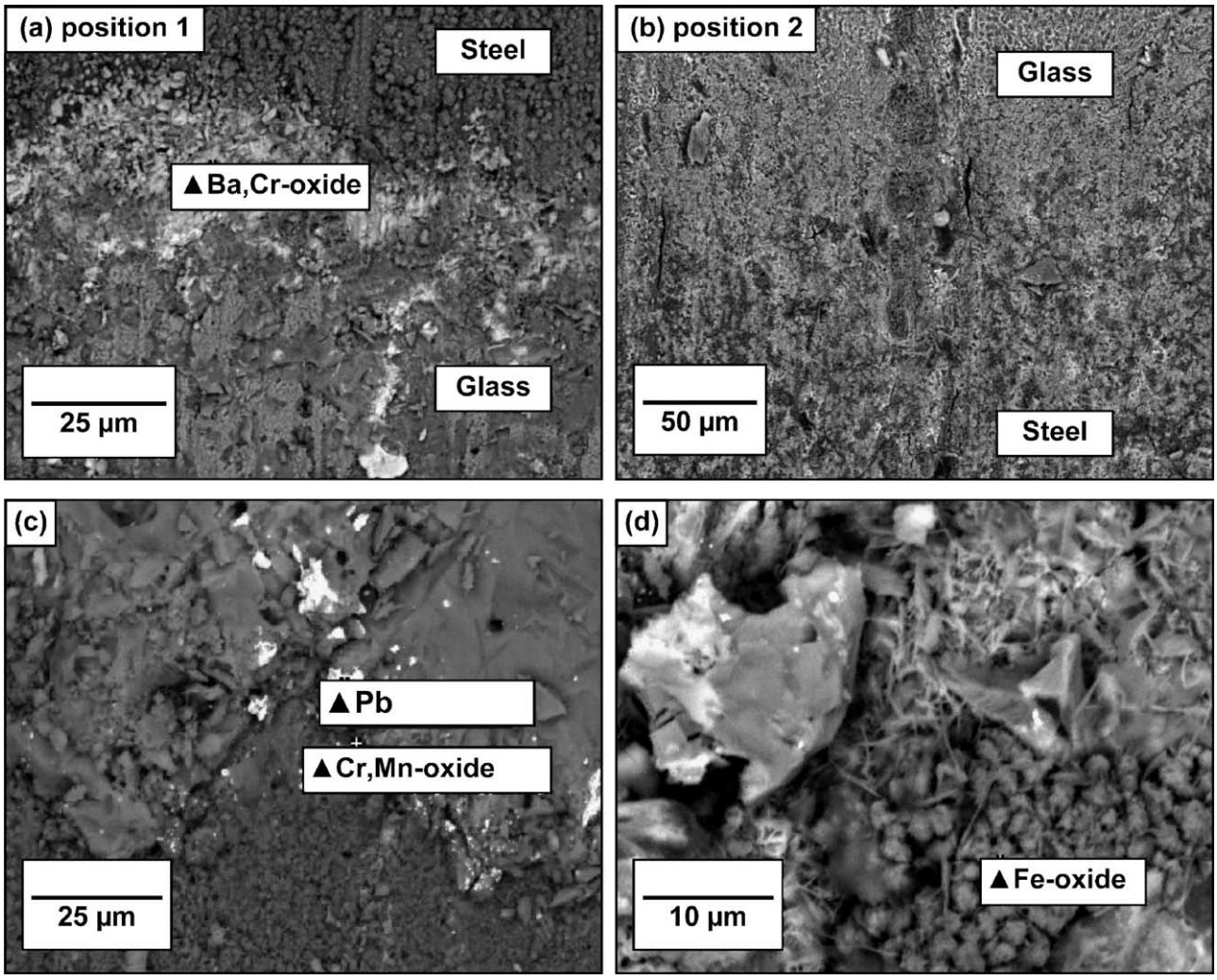

Fig. 11. SEM micrographs of the surface morphology of specimen T7–G73 after exposure for 400 h at 800 °C in a dual atmosphere of hydrogen/air with an externally applied voltage of 800 mV: (a) triple phase boundary air/glass–ceramic sealant/steel (position 1); (b) triple phase boundary hydrogen/glass–ceramic sealant/steel (position 2); (c) higher magnification of the steel surface on the air-side; (d) higher magnification of the steel surface on the hydrogen side.

glass–ceramic, and the steel. After prolonged exposure times it is also found locally near the interface between the glass–ceramic and the steel. In these cases, however, no voluminous external Fe-oxides are formed.

- Neither the voluminous external Fe-oxide formation nor the excessive internal oxidation of Cr is found if the exposures of the samples are carried out in air instead of a dual atmosphere [17].
- If the exposures are carried out in a hydrogen/water vapour mixture instead of a dual atmosphere, the internal oxidation of Cr at the boundary between the environment, the glass–ceramic, and the steel is similar to that described above. However, no voluminous external Fe-oxide formation is found and no short-circuiting occurs [17].
- The excessive internal oxidation of chromium, sometimes accompanied by voluminous, external Fe-oxide formation, only occurs in case of glass–ceramics G73 and G75, i.e. glass–ceramics containing minor amounts of PbO.
- The rate of corrosion attack strongly depends on the detailed steel composition. Increasing Si content apparently increases the rate of the corrosion attack which, in a dual atmosphere, eventually results in short-circuiting (Fig. 15).

Based on these findings in combination with the morphological features of the corrosion products and the time dependence of the reactions, the following sequential steps are proposed to explain the occurrence of the short-circuiting phenomenon:

- In the hydrogen/water vapour environment the remaining PbO in the glass–ceramic will be reduced to Pb because the oxygen partial pressure of the environment is lower than the dissociation pressure of PbO (for $a_{Pb} = 1$ at 800 °C, $\log(pO_2/\text{bar}) = -11$). Due to its low melting point (328 °C) it is obvious that Pb will be present in liquid rather than in solid form. Additionally, substantial amounts of vapour

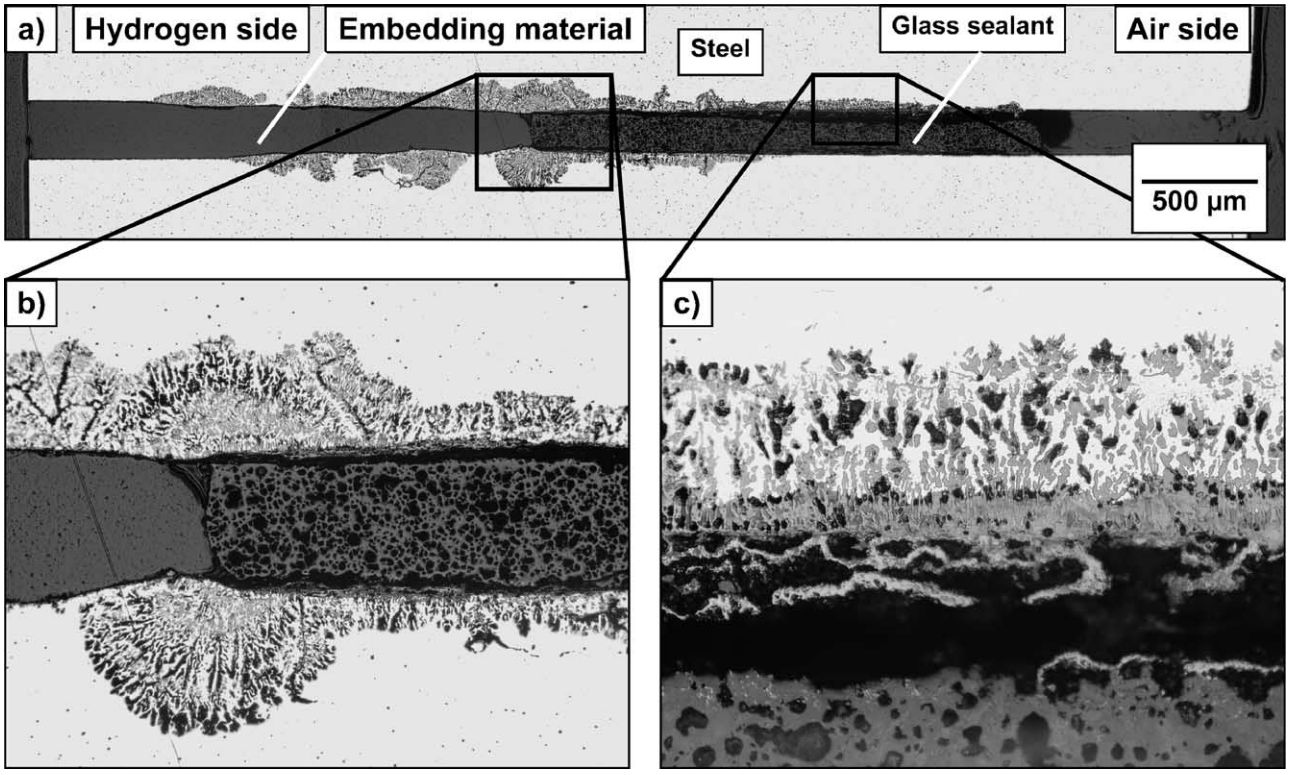

Fig. 12. Optical micrographs of a cross-section of specimen T1–G75 exposed for 400 h at 800 °C in a hydrogen/air dual atmosphere.

phase will be present due to the relatively high vapour pressure of Pb (1×10^{-4} bar at 800 °C).

- At high temperatures a reduction–oxidation reaction takes place between chromium (in the bulk material) and PbO. This explains the presence of small elemental Pb drops along the glass–ceramic/steel interface.
- The internal grain boundary attack of the steels exhibits a morphology which is very similar to that frequently described in the literature as "liquid metal corrosion" [18–20], here likely initiated by liquid Pb at the steel grain boundaries (Fig. 16a and b). The attack makes the grain boundaries accessible for gaseous species such as water vapour, resulting in excessive internal oxidation of chromium. Because of the low melting point and high vapour pressure (vapour phase transport), it is likely that the Pb attack may not only occur in the immediate vicinity of the boundary between the hydrogen-based environment and the glass but also at a small distance from the

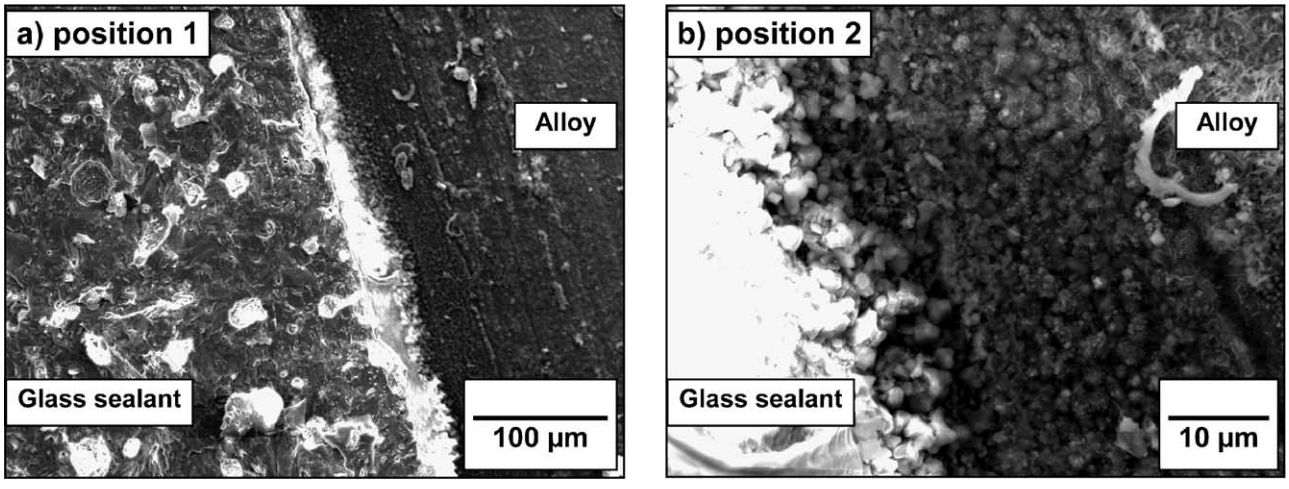

Fig. 13. SEM micrographs of the surface morphology of specimen T1–G76 after exposure for 400 h at 800 °C in a dual atmosphere of hydrogen/air with an externally applied voltage of 800 mV: (a) triple phase boundary air/glass–ceramic sealant/steel (position 1); (b) triple phase boundary hydrogen/glass–ceramic sealant/steel (position 2).

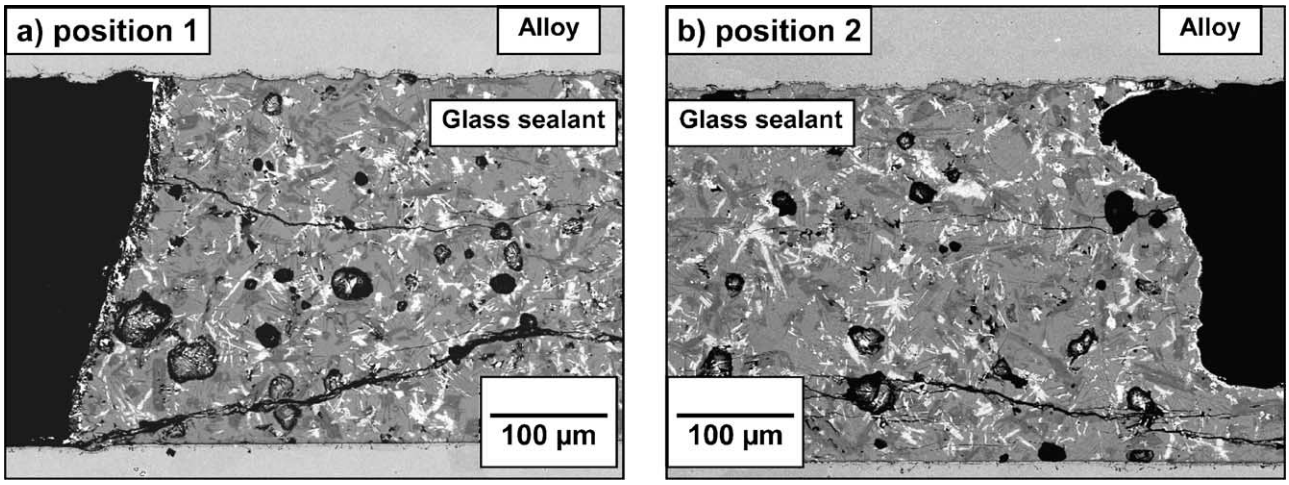

Fig. 14. SEM micrograph of a cross-section of specimen T1–G76 exposed for 400 h at 800 °C in a hydrogen/air dual atmosphere: (a) position 1: air-side; (b) position 2: hydrogen side.

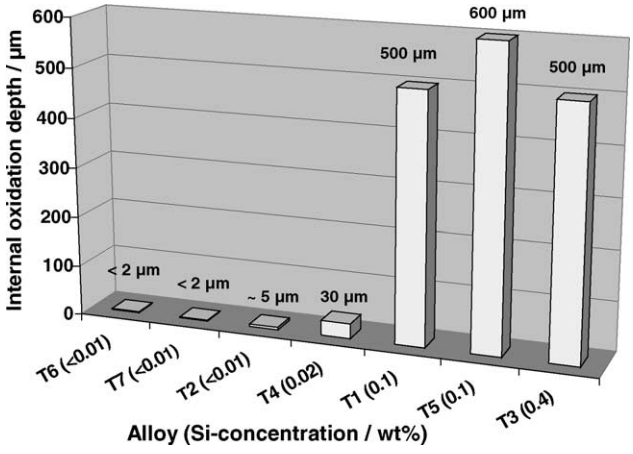

Fig. 15. Internal oxidation depth as a function of the Si concentration of various chromia-forming ferritic steels. Glass–ceramic sealant used: G73; exposure time: 400 h; temperature: 800 °C; atmosphere: hydrogen/air; external voltage applied: 800 mV.

glass–ceramic edge, in agreement with the actual experimental findings (Fig. 12).

- The excessive internal oxidation of Cr, initiated on the hydrogen-based side of the sandwich sample results in a volume change of the ferritic steel, which leads to a local bulging of the steel. As a consequence, the glass–ceramic is pushed away from the steel surface and crack formation at/near the interface between the glass–ceramic and steel occurs (Fig. 16c). This explains the increase in resistance before the onset of short-circuiting (Fig. 2).
- The hydrogen-based gas can penetrate into the crack leading here to the occurrence of local internal oxidation of Cr in a manner similar to that initially started near the edge of the glass–ceramic. Also here, elemental Pb is available along the interface, due to the redox reaction between chromium in the bulk phase and PbO. The crack tip propagates and once the crack reaches the air-side, internal oxidation of Cr also occurs at the boundary between air, glass–ceramic, and steel (Fig. 16d).
- The excessive internal oxidation leads to a severe Cr depletion in the steel matrix. Once the matrix concentration has

Table 4
Schematic overview of phenomena related to various glass–ceramic sealant–steel combinations exposed in a dual atmosphere (hydrogen–air) for 400 h at 800 °C

Steel	T1	T2	T3	T4	T5	T6	T7
Glass–ceramic sealant							
G73	SC: yes IO: +++ EO: +++	SC: no IO: – EO: –	SC: yes IO: +++ EO: +++	SC: no IO: + EO: +++	SC: yes IO: +++ EO: +++	SC: no IO: – EO: –	SC: no IO: – EO: –
G75	SC: yes IO: +++ EO: +++						
G76	SC: no IO: – EO: –						

SC: short-circuiting; IO: internal oxidation along grain boundaries; EO: external oxidation by outwardly growing iron-rich oxide nodules; (–) negligible; (+) small; (++) moderate; (+++) severe.

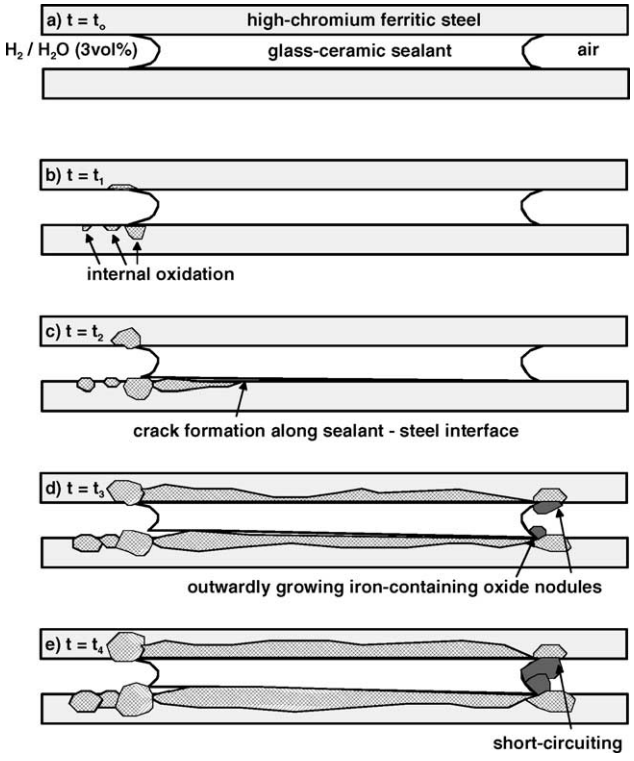

Fig. 16. Schematic illustration of excessive reactions of a sandwich sample with a Si-containing steel and a glass–ceramic sealant including a minor amount of PbO, in a dual atmosphere. Experimental conditions: temperature: 800 °C; hydrogen/air; externally applied voltage 800 mV.

decreased below a critical level the steel is no longer able to retain a protective chromia layer and consequently it will start to form an external Fe-based oxide scale, depending on the pO_2. Due to the low oxygen partial pressure near the glass/steel interface on the hydrogen side, iron will not oxide at all [21]. However, very rapidly growing, external Fe-based oxide scales will be formed near the glass/steel interface on the air-side. This rapid formation of large Fe-oxide nodules will, after prolonged exposure times lead to "bridge"-formation between the two metallic sheets (Fig. 16d and e), and as a result, to short-circuiting.

One might speculate that the transport of hydrogen to the air-side could also occur via a different path to that described above. It is well known that hydrogen can easily permeate through most metallic materials at high temperatures and in this way can affect oxidation processes in dual environment exposures [22–24]. However, previous studies [25,26] have shown that hydrogen permeation through chromia-forming materials is significantly reduced by the presence of the protective oxide layer. This suggests that the contribution of hydrogen permeation by through-metal permeation is likely to be of minor significance in the initiation of the excessive internal Cr oxidation near the interface between glass–ceramic, steel and air. Also on the basis of the morphological features observed in the present study, a transport via the formed cracks along the steel/glass interface is a far more likely process.

The prevailing results strongly indicate that the rate of excessive internal Cr oxidation, which is the "trigger" for the eventual occurrence of short-circuiting in the case of the Pb-containing glass–ceramics is affected by the Si content of the steel. Recent developments of ferritic steels for SOFC interconnects were based on the alloy system FeCrMn (La/Ti) [14 and references therein]. The concentrations of common impurities such as Si and Al were kept as low as technologically possible, because especially Si additions are known to adversely affect the SOFC-relevant properties of the protective Cr-based oxide scale. First, Si easily oxidises internally near the alloy/chromia interface, which may result in a decrease of the electrical conductivity of the oxide scale [15] and/or the scale spallation resistance [15,16,27–31]. Additionally, the volume change caused by internal oxidation leads to outward metal movement resulting in micro-damaging of the scale as well as formation of metallic in-scale inclusions [14,16]. These processes result in a deterioration of the protective scale properties and in an increase of the growth rate of the Cr-based oxide scale [16]. These factors may be responsible for the observed differences in enhanced attack of the various steels by the Pb-containing glass–ceramics. It is, however, difficult to understand why such a process in which internal oxidation deteriorates the protective properties of the external oxide scale would occur in the case of internal oxidation of Si and not in the case of internal oxidation of, for example Al (see Fig. 2c and Table 4). The latter clearly occurs for instance in case of alloys T2 and T4, however these materials showed much slower rates of internal Cr oxidation than Si-containing steels such as T1, T3, and T5. This might indicate that the Si acts in a direct way to promote the internal oxidation attack of the steel grain boundaries making these boundaries permeable for oxygen or water vapour. Further studies will, however, be required to elucidate the detailed effect of minor, oxygen-active alloying additions, especially Si, on the observed detrimental interaction between the Pb-containing glass and high-Cr ferritic steels.

An open question remains, in how far the use of the mentioned glass–ceramics may lead to similar effects as described in the present paper, in other SOFC systems, which are, e.g. designed to operate in the temperature range 900–1000 °C. Considering the mechanisms derived, one might expect that an increase of the operating temperature will even enhance the already observed rapid degradation phenomena because the vapour pressure of Pb will obviously increase with increasing temperature. However, higher temperatures might alter the gas permeability of the surface oxide scales in a negative but also in a positive manner. In the latter case the degradation phenomena would, on the basis of the proposed mechanisms, be expected to decrease because the access of the Pb vapour to the metal surface would be hampered. Improvement of gas tightness of surface oxide scales upon temperature increase have been discussed in literature, however, it would presently

be speculative to derive whether such an effect might occur for the ferritic steels used in the present study. Another complicating factor is that for SOFC systems operating in the temperature range 900–1000 °C, other types of metallic materials, e.g. Cr-base alloys [14] rather than ferritic steels are likely to be used as interconnect materials. Due to their completely different composition in respect to main as well as minor alloying additions as well as major differences in alloy microstructure, a reliable prediction of their behaviour in contact with the discussed (Pb-containing) glass–ceramics seems not possible on the basis of the prevailing results.

5. Conclusions

The present study emphasises that the evaluation of suitable combinations of glass–ceramic sealants and steels for SOFC applications requires the use of realistic test methods which closely simulate the conditions prevailing in actual SOFC stacks. During high-temperature exposure of various glass–ceramic/steel combinations under purely oxidising conditions (air) no severe interactions detrimentally affecting the electrical properties of the sandwich specimens were observed [17]. However, when using experimental parameters which closely simulate SOFC stack conditions, i.e. in the presence of a dual atmosphere, excessive corrosion of the ferritic interconnector steel may occur, which eventually results in a short-circuiting between adjacent interconnector plates.

The “trigger” for this process clearly starts on the side of the sandwich specimen which is in contact with the hydrogen/water vapour environment. Here, the reduction of PbO in the glass–ceramic induces an excessive internal oxidation of chromium. This results in a local volume change of the ferritic steel, which is manifested in bulging of the steel. As a consequence, the glass–ceramic is pushed away from the steel surface and crack formation at/near the glass–ceramic–steel interface occurs. In this way the process “spreads” along this interface to the air-side of the sandwich sample where the resulting chromium depletion of the alloy matrix is accompanied by formation of rapidly growing, external Fe-based oxides. The rate of this corrosion attack strongly depends on the detailed steel composition. Increasing Si content apparently increases the rate of the corrosion attack, which eventually results in short-circuiting.

Acknowledgements

The authors would like to thank the Central Department of Technology (Forschungszentrum Jülich GmbH, Germany), in particular Mr. A. Cramer for preparation of the sandwich samples. In addition, the authors gratefully acknowledge Dr. P. Batfalsky, Dr. D. Sebold, and Dr. E. Wessel for their assistance in SEM sample preparation and analysis.

References

[1] T. Schwickert, P. Geasee, A. Janke, U. Diekmann, R. Conradt, Electrically insulating high-temperature joints for ferritic chromium steel, in: Proceedings of the International Brazing and Soldering Conference, Albuquerque, New Mexico, 2000, pp. 116–122.
[2] K.L. Ley, M. Krumpelt, R. Kumar, J.H. Meiser, I. Bloom, J. Mater. Res. 11 (6) (1996) 1489–1493.
[3] K. Eichler, G. Solow, P. Otschik, W. Schaffrath, BAS ($BaO{\cdot}Al_2O_3{\cdot}SiO_2$)-glasses for high temperature applications, J. Eur. Ceram. Soc. 19 (1999) 1101–1104.
[4] Z. Yang, J.W. Stevenson, K.D. Meinhardt, Solid State Ionics 160 (2003) 213–225.
[5] K.D. Meinhardt, J.D. Vienna, T.R. Armstrong, L.R. Pederson, U.S. Patent 6,430,966 (2002).
[6] S.B. Sohn, S.Y. Choi, G.H. Kim, H.S. Song, G.D. Kim, Stable sealing glass for planar solid oxide fuel cell, J. Non-Cryst. Solids 297 (2002) 103–112.
[7] T. Schwickert, R. Sievering, P. Geasee, R. Conradt, Mat.-Wiss. U. Werkstofftech. 33 (2002) 363–366.
[8] P. Geasee, Doctoral Thesis, RWTH Aachen, Germany, 2003.
[9] Z. Yang, K.S. Weil, D.M. Paxton, J.W. Stevenson, J. Electrochem. Soc. 150 (9) (2003) A1188–A1201.
[10] N.H. Menzler, D. Sebold, M. Zahid, S.M. Gross, Th. Koppitz, Interaction of metallic SOFC interconnect materials with glass–ceramic sealant in various atmospheres, J. Power Sources, in press.
[11] V.A.C. Haanappel, V. Shemet, I.C. Vinke, W.J. Quadakkers, A novel method to evaluate the suitability of glass sealant–alloy combinations under SOFC stack conditions, J. Power Sources 141 (2005) 102–107.
[12] W.J. Quadakkers, in: N.H. Afghan, M. da Graça Carvalho (Eds.), Proceedings of the New and Renewable Technologies for Sustainable Development, Madeira Island, Portugal, June 26–29, Kluwer Academic Publishers, Boston, 2002, pp. 391–398.
[13] W.J. Quadakkers, T. Malkow, J. Piron-Abellan, U. Flesch, V. Shemet, L. Singheiser, in: A. McEvoy (Ed.), Proceedings of the 4th European SOFC Forum, Lucerne, Switzerland, July 10–14, 2000, pp. 827–836.
[14] W.J. Quadakkers, J. Piron-Abellan, V. Shemet, L. Singheiser, Mater. High Temp. 20 (2) (2003) 115–127.
[15] E. Konycheva, J. Laatsch, E. Wessel, F. Tietz, N. Christiansen, L. Singheiser, K. Hilpert, in: M. Mogensen (Ed.), Proceedings of the 6th European SOFC Forum, Lucerne, Switzerland, June 28–July 2, 2004, pp. 1586–1593.
[16] P. Huczkowski, N. Christiansen, V. Shemet, L. Singheiser, W.J. Quadakkers, in: M. Mogensen (Ed.), Proceedings of the 6th European SOFC Forum, Lucerne, Switzerland, June 28–July 2, 2004, pp. 1594–1601.
[17] V.A.C. Haanappel, V. Shemet, I.C. Vinke, S.M. Gross, Th. Koppitz, N.H. Menzler, M. Zahid, W.J. Quadakkers, Evaluation of the suitability of various glass sealant–steel combinations under SOFC stack conditions, J. Mater. Sci., in press.
[18] V.Y. Abramov, S.N. Bozin, S.V. Evropin, B.S. Rodchenkov, V.N. Leonov, A.I. Filin, Proceedings of the 11th International Conference on Nuclear Engineering, Tokyo, Japan, April 20–23, 2003, ICONE11-36413, pp. 1–4.
[19] G. Benamati, C. Fazio, H. Piankova, A. Rusanov, J. Nucl. Mater. 301 (2002) 23–27.
[20] V.E. Fradkov, Scripta Metall. Mater. 30 (12) (1994) 1599–1603.
[21] J. Zurek, M. Michalik, L. Singheiser, W.J. Quadakkers, Oxidation Met., in press.
[22] I.L. Tazhibaeva, A.Kh. Klepikov, O.G. Romanenko, V.P. Shestakov, Fusion Eng. Design 51–52 (2000) 199–205.
[23] W. Song, J. Du, Y. Xu, B. Long, J. Nucl. Mater. 246 (1997) 139–143.
[24] P. Jung, J. Nucl. Mater. 238 (1996) 189–197.

[25] Z. Yang, M. Walker, G. Xia, P. Singh, J.W. Stevenson, Anomalous corrosion behavior of stainless steels under SOFC interconnect exposure conditions, Electrochem. Solid-State Lett. 6 (10) (2003) B35–B37.
[26] K. Nakagawa, Y. Matsunaga, T. Yanagisawa, Corrosion behavior of ferritic steels on the air-sides of boiler tubes in a steam/air dual environment, Mater. High Temp. 18 (1) (2001) 51–56.
[27] J.S. Dunning, D.E. Alman, J.C. Rawers, Oxidation Met. 57 (5–6) (2002) 409–425.
[28] B. Ahmad, P. Fox, Oxidation Met. 52 (1–2) (1999) 113–138.
[29] S.N. Basu, G.J. Yurek, Oxidation Met. 36 (3–4) (1991) 281–315.
[30] D.J. Baxter, R.C. Hurst, R.T. Derricott, Werkstoffe und Korrosion 35 (6) (1984) 266–272.
[31] J.C. Rawers, E.M. Mattlin, Metall. Trans. A 18A (10) (1987) 1805–1812.